Valence band electronic structure of $Pr_{1-x}Sr_xMnO_3$ from photoemission studies

2005 J. Phys.: Condens. Matter 17 2993

(http://iopscience.iop.org/0953-8984/17/19/013)

INSTITUTE OF PHYSICS PUBLISHING JOURNAL OF PHYSICS: CONDENSED MATTER

J. Phys.: Condens. Matter **17** (2005) 2993–2999 doi:10.1088/0953-8984/17/19/013

Valence band electronic structure of $Pr_{1-x}Sr_xMnO_3$ from photoemission studies

P Pal[1], M K Dalai[1], B R Sekhar[1], S N Jha[2], S V N Bhaskara Rao[2], N C Das[2], C Martin[3] and F Studer[3]

[1] Institute of Physics, Sachivalaya Marg, Bhubaneswar, India
[2] Spectroscopy Beamline, INDUS-I, Centre for Advanced Technology, Indore-452013, India
[3] Laboratoire CRISMAT, UMR 6508, ISMRA, Boulevard du Marechal Juin, 14050 Caen, France

E-mail: sekhar@iopb.res.in

Received 18 December 2004, in final form 15 March 2005
Published 29 April 2005
Online at stacks.iop.org/JPhysCM/17/2993

Abstract

We have studied the charge carrier doping dependent changes in the valence band electronic structure of the $Pr_{1-x}Sr_xMnO_3$ system across the orbital ordered compositions using ultraviolet photoelectron spectroscopy. The $d_{x^2-y^2}$ orbital ordering is found to be causing an enhancement of the Mn 3d–O 2p hybridization strength and thereby the Mn 3d contribution to the subbands in the valence region. Our photoemission studies using different photon energies help in elucidating the nature and composition of the valence band features.

1. Introduction

The electronic structure of manganites with general composition $RE_{1-x}A_xMnO_3$ (RE = rare earth, A = alkaline earth) exhibiting colossal magnetoresistance (CMR) properties has been a field of immense interest since their discovery [1, 2]. Properly doped compounds of this Mn^{3+}/Mn^{4+} mixed valent system show a ferromagnetic metallic behaviour at low temperatures and a paramagnetic insulating behaviour at high temperatures. The temperature and doping dependent metal–insulator transitions in these materials are found to be closely related to the unique electronic structure derived from the Mn 3d and O 2p hybridized orbitals [3]. The 3d orbitals of Mn in the MnO_6 octahedra, which are split by the crystal field into low-lying t_{2g} and e_g states, are further split by the Jahn–Teller distortion. The double-exchange (DE) model [4–6] says that the itinerant, doped charge carriers (Mn^{4+} species or e_g holes) mediate between the localized t_{2g} spins and cause the increase in the mobility of the charge carriers. However, recent progress in experimental and theoretical work has brought the realization that the DE model is insufficient to explain all the properties of these CMR materials [7–10], particularly the high-resistivity behaviour above the transition temperature T_c [11].

Undoped parent compounds of these materials, like $LaMnO_3$ and $PrMnO_3$ (so-called A-type antiferromagnetic (AFM) insulators), show a strong interplay between spin and orbital

ordering originating from the single occupancy of the doubly degenerate e_g orbitals of Mn^{3+} ions. With charge carrier doping at the A-site, many of them show well defined orbital ordering (OO) and/or charge ordering (CO) at low temperatures, especially when x equals a commensurate value [12] (e.g. $x = 0.5$). It is still an open question whether or not the OO state with ordered e_g orbitals of Mn^{3+} ions and the CO state with the Mn^{3+} ($t_{2g}^3 e_g^1$) and Mn^{4+} (t_{2g}^3) ions arranged as in a chequerboard occur simultaneously at low temperatures [13]. Anyway, the CO state was found to have a strong influence on the one-electron bandwidth (W) of the e_g band [14] and the transfer interaction of the e_g holes (electrons). The structural origin of these orderings in most of the materials is found to be the $GdFeO_3$-type lattice distortion of the MnO_6 octahedra in the perovskite structures. Such lattice distortions are governed by a tolerance factor [15] which depends on the A-site cation radius. As the cation radius decreases, the Mn–O–Mn bond angle deviates from 180°, thereby decreasing the effective d-electron hopping interaction or W. Since this bond angle change determines the exchange coupling between the Mn^{3+} and Mn^{4+} sites, which in turn depend on the occupation of the e_g orbital, the orbital degrees of freedom are very important in these systems [16, 17]. $La_{0.5}Sr_{0.5}MnO_3$ and $Nd_{0.5}Ca_{0.5}MnO_3$ are two typical examples of extreme cases of such a distortion, with the former least distorted and the latter strongly distorted. Among these compounds, showing an OO and/or CO state at low temperatures, $Pr_{1-x}Sr_xMnO_3$ is of special significance due to its moderate lattice distortion [18] and its A-type AFM ordering at 50% hole doping [19]. Though the orbital ordering in this compound has been observed in diffraction experiments [19, 20], charge ordering has not yet been corroborated after an early report [21]. Nevertheless, unlike other OO/CO CMR materials, $Pr_{1-x}Sr_xMnO_3$ shows a nearly degenerate ferromagnetic metallic state and CO insulating state with a field-induced phase transition possible between them [14]. Interestingly, the orbital ordering in this compound is where the Mn^{3+} ions are expanded and the Mn^{4+} ions are contracted within the c-plane of the structure. Owing to such a strong influence on the electronic structure, the OO phenomena in these materials could provide a wealth of spectroscopic information.

Photoelectron spectroscopy is a very powerful experimental tool at the forefront of physics and materials research, which can directly probe the most crucial low energy spectral weight changes near the Fermi level (E_F). Using this technique, in this study we probed the normal state changes in the valence band electronic structure with charge carrier doping in the $Pr_{1-x}Sr_xMnO_3$ system where the insulator–metal transition takes place around $x = 0.25$ and an orbital ordering sets in around $x = 0.5$ at lower temperatures. In order to understand the nature of the valence band features, particularly the occupied states of t_{2g} and e_g spins and their contributions to the density of states (DOS) near E_F, we used different energies for photoelectron excitation in this study.

2. Experimental details

The $Pr_{1-x}Sr_xMnO_3$ samples we used in this study were polycrystalline in nature and were prepared by solid state reactions. Stoichiometric amounts of Pr_6O_{11}, $SrCO_3$ and MnO_2 were thoroughly mixed and heated at 1000 °C for 24 h. Sr rich samples, at this stage, were heated at the same temperature under Ar atmosphere. The powders pressed in the form of pellets were then heated at 1500 °C for 12 h and slowly cooled down to room temperature in Ar flow. These pellets were annealed at 600 °C for 12 h under oxygen pressure. Precautions had been taken to obtain a single cubic-like perovskite phase, without hexagonal polytype defects. The monophasic and homogeneous compositions of the samples were confirmed using x-ray diffraction measurements, iodometric titration and energy dispersive spectroscopy

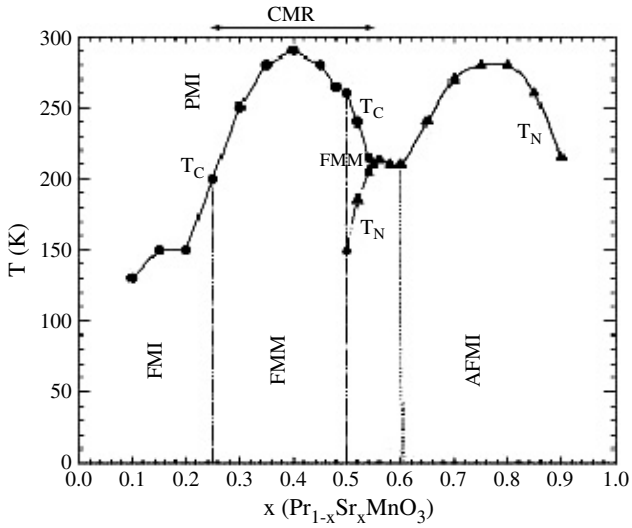

Figure 1. The phase diagram of $Pr_{1-x}Sr_xMnO_3$ system determined from four-probe resistivity, SQUID magnetometry and structural studies [20].

analyses. Resistive and magnetic behaviour of the samples have been studied using the four-probe technique and SQUID magnetometry. Details of the sample preparation, characterization and structural studies are published elsewhere [20, 22, 23]. Figure 1 shows the phase diagram derived from all the above-mentioned studies. Out of the whole series of $Pr_{1-x}Sr_xMnO_3$ we have chosen four samples with compositions $Pr_{0.7}Sr_{0.3}MnO_3$, $Pr_{0.5}Sr_{0.5}MnO_3$, $Pr_{0.4}Sr_{0.6}MnO_3$ and $Pr_{0.2}Sr_{0.8}MnO_3$, which at low temperatures show ferromagnetic metallic, orbital ordered and antiferromagnetic insulating behaviours.

Angle integrated valence band photoemission measurements were performed at the BARC beamline of the Indus-I synchrotron radiation source where toroidal grating monochromators were used to select the photon energies from the bending magnet radiation. Photon flux was of the order of 10^{10} photons s^{-1} with a beam size of 1.5×1 mm^2. A hemispherical analyser was used to measure the kinetic energy of the photoelectrons inside the ultra-high vacuum (UHV). In this study we used two different photon energies, 130 and 200 eV, for which the overall resolution was ∼150 meV. All measurements were performed at room temperature. The polycrystalline samples were scraped *in situ* using a diamond file, where the base pressure of the vacuum chamber was around 10^{-10} mbar. Scraping was repeated many times until negligible intensity was found for the ∼10 eV binding energy peak, which is due to surface contamination [24] and is commonly found in polycrystalline pellet samples of transition metal oxide compounds. The binding energies of our photoemission spectra are referenced to the Fermi level (E_F) step recorded on a clean platinum foil kept in electrical and thermal contact with the samples.

3. Results and discussion

In figure 2 we present the normalized valence band photoemission spectra of the $Pr_{1-x}Sr_xMnO_3$ samples with $x = 0.3$, 0.5, 0.6 and 0.8 taken at a photon energy of 130 eV. The spectra consist of two prominent features, one near E_F at ∼3.3 eV (marked B) and another at ∼5.7 eV (marked C), both arising from the Mn 3d–O 2p hybridized states [25]. At 130 eV photon

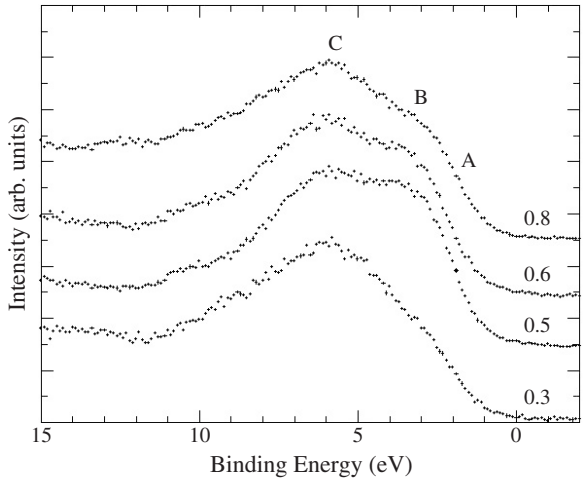

Figure 2. The valence band photoemission spectra of $Pr_{1-x}Sr_xMnO_3$ samples taken using 130 eV energy photons. Features A, B and C have major contributions from $e_{g\uparrow}$, $t_{2g\uparrow}$ and $e_{g\uparrow} + t_{2g\uparrow}$ states.

energy, the emission spectra should be dominated by O 2p states due to their higher cross section compared to Mn 3d [26]. Besides the two features, a close observation will reveal the presence of a very low-intensity shoulder (marked A) close to (∼1.5 eV) E_F. Band structure calculations based on the local spin-density approximation [27] on $Pr_{0.5}Sr_{0.5}MnO_3$ and configuration-interaction analysis of MnO_6 clusters in La–Sr–MnO [3, 28] have ascribed the highest subband A, at the top of the valence band, to the $e_{g\uparrow}$ states, and subband B to $t_{2g\uparrow}$ states, while C is a mixture of $t_{2g\uparrow}$ and $e_{g\uparrow}$ states. It should also be noticed from our spectra (figure 2) that the width of the valence band (features A, B and C together) changes with increase in Sr doping. The widths of the spectra from the samples with $x = 0.5$ and 0.6 are increased by 0.4 and 0.7 eV respectively compared to the width from $x = 0.3$, while $x = 0.8$ shows only a 0.3 eV increase.

In order to see the contributions of different states to the features we have taken the valence band spectra of the same set of samples at a higher photon energy of 200 eV. The spectra showed a decreased intensity for both features B and C. Figure 3 shows both the spectra taken at 130 and 200 eV. In this plot, each pair of spectra was normalized in intensity at E_F and all along the 15–25 eV binding energy region. The figure shows a larger decrease in the intensity of B and C for both $x = 0.3$ and 0.8 samples. Interestingly, the spectra corresponding to $Pr_{0.5}Sr_{0.5}MnO_3$ shows only a very slight decrease in the intensities of these features compared to the other samples. Intensity changes for $x = 0.6$ are also smaller compared to those from the 30% and 80% doping. Though the feature marked A in the spectra has a significant role in CMR properties, the changes in its intensity are not very clear from the spectra at different photon energies due to the very low density of these states. In general, for hole doped CMR compounds the intensity of this feature is expected to decrease with increase in Sr doping, depicting the decrease in the $e_{g\uparrow}$ states as the composition approaches $SrMnO_3$ (t_{2g}^3). Keeping in mind the fact that the intensity variations observed in features B and C could be more prominent at lower photon energies, we have taken the valence band spectra of all these samples at 20, 40 and 90 eV. Although, due to the technical limitations of our monochromator, quality and statistics of our raw spectra were not very good, they also showed very similar trends in intensity changes as in the spectra using 130 and 200 eV.

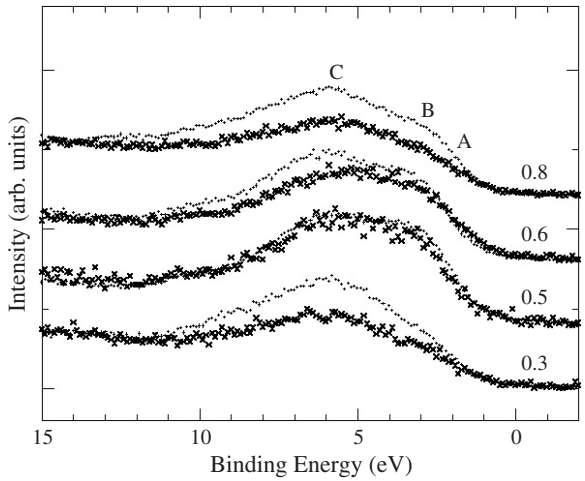

Figure 3. The valence band photoemission spectra of $Pr_{1-x}Sr_xMnO_3$ samples taken using $h\nu = 130$ and 200 eV plotted together. Intensities of each pair of spectra were normalized at E_F and all along the 15–25 eV binding energy region.

An obvious observation from the above-mentioned spectral weight changes, as a function of charge carrier doping or photon energy variation, is that the samples with $x = 0.5$ and 0.6 behave differently from other compositions. The $x = 0.3$ sample has a ferromagnetic metallic phase at low temperatures and shows CMR properties (see figure 1). On the other hand, $Pr_{0.2}Sr_{0.8}MnO_3$ shows an antiferromagnetic insulating behaviour below the transition temperature. $Pr_{0.5}Sr_{0.5}MnO_3$ with its A-type antiferromagnetic structure and $d_{x^2-y^2}$ orbital ordering [19, 29] below the T_N has a unique behaviour of two magnetic transitions i.e. paramagnetic insulating to ferromagnetic metallic to antiferromagnetic insulating [20]. As mentioned earlier, the latter two states are nearly degenerate [14]. Hartree–Fock calculations on the La–Sr–Mn–O system have shown the A-type AFM CO state with $d_{x^2-y^2}$ orbital ordering has the lowest energy [30]. With this orbital ordering the e_g electrons of the Mn^{3+} ions are accommodated in the $x^2 - y^2$ orbitals. Since the exchange coupling between the Mn^{3+} and Mn^{4+} depends on which type of orbital is occupied at the Mn^{3+} site, the valence band features depend grossly on the orbital ordering. The orbital ordering and occupation in the sample with $x = 0.6$ should be quite closer to those of $x = 0.5$, though this sample ($Pr_{0.4}Sr_{0.6}MnO_3$) has no metallic state at low temperature. The similarity can be seen in the magnetic phase diagram shown in figure 1. As the doped hole concentration x increases beyond 60% the AFM insulating state becomes stable with a possible change of the AFM structure from A type to CE type. The low-temperature insulating behaviour of $x = 0.8$ sample has been reported to be due to such an orbital ordering and resulting charge localization [20].

Keeping these structural aspects in mind one can understand the observed changes in the valence band electronic structure of these samples. Though this study has been done at 300 K where all the samples are above their transition temperature, the energy positions of the spectral features generally remain similar to those from photoemission studies performed at temperatures below the sample's transition. Prominent temperature dependent changes were earlier found in the intensities of feature B and those spin states close to E_F due to the e_g electrons [28, 25]. The observed spectral weight changes in our study are in correspondence with these temperature dependent changes. This again is consistent with the observation that

increasing the charge carrier concentration x and decreasing the temperature have similar effects in this system of materials [25].

With the increase in charge carrier concentration from $x = 0.3$ to 0.5 (figure 2) we observe an enhancement of the spectral intensity of feature B, which has a contribution from the t_{2g} states of MnO_6 octahedra. This subband must also have O 2p character coming from the Mn 3d–O 2p hybridization. Saito *et al* [25] have shown that this feature has a substantial O 2p non-bonding states contributing to it. Increase in charge carrier concentration may result in the increase of the p–d hybridization strength. In other CMR systems like $La_{1-x}Sr_xMnO_3$ an increase in this strength has been found with more doping [25, 24]. Further, the increase in p–d hybridization and resulting increase in O 2p character has been inferred to be the reason for the increase in the intensity of feature B with lowering of temperature [25, 24]. It is natural to expect that in the $Pr_{1-x}Sr_xMnO_3$ system also the p–d hybridization strength increases with x. However, apart from this, in this system an increase of Sr doping leads to an orbital ordering of $d_{x^2-y^2}$ type. The $d_{x^2-y^2}$ type orbital ordering could strengthen the p–d hybridization further. More importantly, with $d_{x^2-y^2}$ ordering of the Mn 3d orbitals, it is more probable that the contribution of the Mn 3d states increases in feature B. Hence, the enhancement of intensity of subband B as we go from $x = 0.3$ to 0.5 in our spectra (figure 2) could be due to the increase in the Mn 3d character with orbital ordering. This is supported by the fact that intensity of B decreases with further doping. In the sample with 60% charge doping, the intensity of B decreases as the $d_{x^2-y^2}$ orbital ordering and thereby the hybridization weakens beyond $x = 0.5$. Similarly for the last sample, $Pr_{0.2}Sr_{0.8}MnO_3$, the Mn 3d contribution to the feature decreases. Here, structural studies have also shown that the orbital ordering in this sample changes to a d_{z^2} type with CE-type AFM structure [20]. Nevertheless, this sample also shows a higher intensity for feature B compared to $x = 0.3$. The changes in the valence band width with increasing x, as mentioned earlier, could also possibly be due to the extent of orbital ordering and p–d hybridization strength in different samples. Similar increase in the valence band width was earlier observed in the $La_{1-x}Sr_xMnO_3$ system also [25], though the magnitude of the increase was smaller for compositions near to $x = 0.5$ and 0.6.

When we move on to figure 3, the above picture becomes clearer. With change of photon energy, decrease in the intensities of features B and C for the sample with $x = 0.3$ was expected as the contribution of oxygen states to these are high. This is due to the lower photoemission cross section of oxygen states at higher photon energies. Similarly, for the 80% doped sample also we find a dominance of the oxygen states throughout the valence band. Again, the spectrum from $Pr_{0.5}Sr_{0.5}MnO_3$ shows a different behaviour. It shows only a very slight decrease in the intensities of features B and C compared to the other samples. Intensity changes for $x = 0.6$ are also smaller compared to those from the 30% and 80% doped. As we discussed earlier, the $d_{x^2-y^2}$ orbital ordering associated with the 50% doped sample could be the cause for this difference in behaviour. Because of the orbital ordering and increased p–d hybridization, in this compound features B and C could have a dominant Mn 3d contribution. The photoemission cross sections of these Mn states do not vary markedly with changes in photon energy, particularly in this energy range, unlike the O states, so an increase in the photon energy does not make a significant change in intensities for B and C in the sample with $x = 0.5$. $x = 0.6$ also shows a similar behaviour due to the orbital ordering which is still active, though diminished.

The above results show that the valence band electronic structure is intimately connected with the charge/orbital ordering in the $Pr_{1-x}Sr_xMnO_3$ system. The $d_{x^2-y^2}$ orbital ordering and the concomitant increase in the Mn 3d character of the near E_F features of the electronic structure could have a strong influence on the degree of charge carrier localization. In the current scenario, where the unconventional electronic structural properties of CMR systems

with A-type antiferromagnetic coupling is crucially important in understanding the exchange interactions of the e_g electron, these results could provide some insights.

4. Conclusions

The normal state electronic structure of $Pr_{1-x}Sr_xMnO_3$ probed using ultraviolet photoelectron spectroscopy shows doping dependent spectral weight changes similar to the temperature dependent changes in the valence band region. Samples near to the half doped regime were found with enhanced Mn 3d character in their near E_F features. Increase in the Mn 3d–O 2p hybridization strength associated with the A-type antiferromagnetic state with $d_{x^2-y^2}$ type orbital ordering could be the cause of this increase in the 3d character. An experiment using higher photon energy confirms this enhancement.

References

[1] von Helmolt R, Wecker J, Holzapfel B, Schultz L and Samwer K 1993 *Phys. Rev. Lett.* **71** 2331
[2] Tokura Y, Urushibara A, Moritomo Y, Arima T, Asamitsu A, Kido G and Furukawa F 1994 *J. Phys. Soc. Japan* **63** 3931
[3] Saitoh T, Bocquet A E, Mizokawa T, Namatame H, Fujimori A, Abbate M, Takeda Y and Takano M 1995 *Phys. Rev.* B **51** 13942
[4] Zener C 1951 *Phys. Rev.* B **82** 403
[5] Anderson P W and Hasegawa H 1955 *Phys. Rev.* **100** 675
[6] de Gennes P-G 1960 *Phys. Rev.* **118** 141
[7] Millis A J, Littlewood P B and Shraiman B I 1995 *Phys. Rev. Lett.* **74** 5144
[8] Park J H, Vescovo E, Kim H J, Kwon C, Ramesh R and Venkatesan T 1998 *Nature* **392** 794
[9] Picket W E and Singh D J 1996 *Phys. Rev.* B **53** 1146
[10] Toulemonde O, Millange F, Studer F, Raveau B, Park J H and Chen C T 1999 *J. Phys.: Condens. Matter* **11** 109
[11] Rao C N R and Raychaudhuri A K 1998 *Colossal Magnetoresistance, Charge Ordering and Related Properties of Manganese Oxides* ed C N R Rao and B Raveau (Singapore: World Scientific)
[12] Sternlieb B J, Hill J P, Wildgruber U C, Luke G M, Nachumi B, Morimoto Y and Tokura Y 1996 *Phys. Rev. Lett.* **76** 2169
[13] Zimmermann M v *et al* 1999 *Phys. Rev. Lett.* **83** 4872
[14] Tomioka Y, Asamitsu A, Moritomo Y, Kuwahara H and Tokura Y 1995 *Phys. Rev. Lett.* **74** 5108
[15] Tokura Y 1998 *Colossal Magnetoresistance* ed Y Tokura (Singapore: World Scientific)
[16] Goodenough J B 1963 *Magnetism and Chemical Bond* (New York: Interscience)
[17] Khomskii D and Sawatzky G 1997 *Solid State Commun.* **102** 87
[18] Fujimori A, Mizokawa T and Saitoh T 1998 *Colossal Magnetoresistance, Charge Ordering and Related Properties of Manganese Oxides* ed C N R Rao and B Raveau (Singapore: World Scientific)
[19] Kawano H, Kajimoto R, Yoshizawa H, Tomioka Y, Kuwahara H and Tokura Y 1997 *Phys. Rev. Lett.* **78** 4253
[20] Martin C, Maignan A, Hervieu M and Raveau B 1999 *Phys. Rev.* B **60** 12191
[21] Knizek K, Jirak Z, Pollert E, Zounova F and Vratislav S 1992 *J. Solid State Chem.* **100** 292
[22] Martin C, Maignan A, Hervieu M, Raveau B, Jirak Z, Savosta M M, Kurbakov A, Trounov V, Andre G and Bouree F 2000 *Phys. Rev.* B **62** 6442
[23] Hervieu M 2000 *Chem. Mater.* **12** 1456
[24] Sarma D D, Shanti N, Krishnakumar S R, Saitoh T, Mizokawa T, Sekiyama A, Kobayashi K, Fujimori A, Weschke E, Meier R, Kaindl G, Takeda Y and Takano M 1996 *Phys. Rev.* B **53** 6873
[25] Saitoh T, Sekiyama A, Kobayashi K, Mizokawa T, Fujimori A, Sarma D D, Takeda Y and Takano M 1997 *Phys. Rev.* B **56** 8836
[26] Yeh J J and Lindau I 1985 *At. Data Nucl. Data Tables* **32** 1
[27] Kurmaev E Z, Korotin M A, Galakhov V R, Finkelstein L D, Zabolotzky E I, Efremova N N, Lobachevskaya N I, Stadler S, Ederer D L, Callcott T A, Zhou L, Moewes A, Bartkowski S, Neumann M, Matsuno J, Mizokawa T, Fujimori A and Mitchell J 1999 *Phys. Rev.* B **59** 12799
[28] Chainani A, Mathew M and Sarma D D 1993 *Phys. Rev.* B **47** 15397
[29] Damay F, Martin C, Herview M, Maignan A, Raveau B, Andre G and Bouree F 1998 *J. Magn. Magn. Mater.* **184** 71
[30] Mizokawa T and Fujimori A 1997 *Phys. Rev.* B **56** R493